

Highlights

Yellow River Basin Regional Hydrological Modelling with Consideration of Irrigation

Cong Jiang, Eric J. R. Parteli, Xin Yin, Qian Xia, Yaping Shao

- We applied the AHMS to study hydrological processes in the Yellow River Basin.
- Parameter sensitivity and water budget analyses were carried out for AHMS.
- In the absence of irrigation, AHMS underestimates evaporation and overestimates runoff.
- We extended the AHMS to include river water use processes for irrigation.
- AHMS can better simulate the streamflow and evaporation by considering irrigation.

Yellow River Basin Regional Hydrological Modelling with Consideration of Irrigation

Cong Jiang^{a,*}, Eric J. R. Parteli^b, Xin Yin^a, Qian Xia^c and Yaping Shao^a

^a*Institute for Geophysics and Meteorology, University of Cologne, Pohlstr. 3, Cologne, 50969, North Rhine-Westphalia, Germany*

^b*Faculty of Physics, University of Duisburg-Essen, Duisburg, Lotharstr. 1, 47057, North Rhine-Westphalia, Germany*

^c*School of Water Resources and Hydropower Engineering, Wuhan University, Bayi road. 299, 430072, Hubei Province, China*

ARTICLE INFO

Keywords:

AHMS
Yellow River Basin
Irrigation
Offline AHMS simulation
Calibration
Evaluation

ABSTRACT

It has been recognized that intensive human activities, especially irrigation in the arid and semi-arid regions, dramatically affect the hydrological processes. However, the effects of river irrigation in large irrigation districts on hydrological processes in the Yellow River Basin are less well studied. Here, the Atmospheric and Hydrological Modelling System (AHMS) is applied in offline mode to study hydrological processes and the channel routing model is extended to include the water use for irrigation. The model with and without irrigation process is calibrated and evaluated using the in-site observation data and remote sensing data. The comparison of simulated streamflow and station observations shows a significant improvement in AHMS performance when irrigation is considered. The present work demonstrates the capacity of the AHMS for long-term hydrological simulation and the AHMS simulation provide a comprehensive and quantitative overview of the water resources in this important river basin.

Software availability

Software name: AHMS-IRRIG

Developer: Cong Jiang

Hardware requirements: PC, HPC

System requirements: Linux

Program language: Fortran

Availability: <https://github.com/JiangCong1990/AHMS-IRRIG>

License: Free and open source

Documentation: README and guided example in Github repository

1. Introduction

In the past few decades, the development of hydrological models has been an important research topic (Devia et al., 2015). Early surface hydrological models include SHE (Systeme Hydrologique European) (Abbott et al., 1986), TOPMODEL (Beven and Kirkby, 1979), CACS2D (Julien and Saghafian, 1991). A number of land surface models (e.g., NoahMP, CLM, VIC, ALSIS)(Niu et al., 2011; Oleson et al., 2010; Liang et al., 1994; Irannejad and Shao, 1998), hydrodynamic models (e.g., MGB-IPH, Cama-Flood, LISFLOOD-FP, MIKE-Flood)(Collischonn et al., 2007; Yamazaki et al., 2011; Bates and De Roo, 2000; Patro et al., 2009), as well as coupled atmospheric and hydrological modelling systems (e.g., WRF-Hydro, WRF-HMS, TerrsysMP)(Gochis et al., 2013; Wagner et al., 2016a; Shrestha et al., 2014) have been developed to meet various needs. Hydrological models have been used to predict floods, droughts and related natural hazards (Brunner et al., 2021), and to assess regional water resources (Tegegne et al., 2017). Furthermore, hydrological modeling provides a powerful tool to study hydrological processes, such as

*Corresponding author

 c.jiang@uni-koeln.de (C. Jiang)

ORCID(s): 0000-0002-2405-6645 (C. Jiang)

evapotranspiration, soil moisture and groundwater storage, river and floodplain hydrodynamics and sediment transport in surface hydrological systems. Coupled atmospheric and hydrological models can be used to investigate the dynamic feedback between the atmosphere, land surface and subsurface, and finds applications in climate change and land-use change studies (Wilby et al., 1994; Maxwell et al., 2007).

Hydrological simulation is more challenging for arid and semi-arid regions than for humid regions (Pilgrim et al., 1988) because of the usually low and heterogeneous rainfall, intermittent river flow and fragile environment which is sensitive to human activities. The Yellow River Basin is selected as the research area owing to the unique hydrological characteristics and important position in China. The Yellow River is the second-longest river in China (5464 km) and the Yellow River Basin (795,000 km²) is the largest basin in north China. The average water resources in the Yellow River Basin account for only 2 % of the total water resources in China, but it feeds 12 % of the Chinese population. The shortage of water has led to the conflict between the water supply and demand in this area with continuing population growth and urban development. In 1997, the downstream 704 kilometers from the estuary dried up for more than 226 days (Cong et al., 2009). As large irrigation districts in the Yellow River Basin are mainly located in arid and semi-arid areas, irrigation accounts for more than 80% of the gross human water use from 1956 to 2000 (Fig. 1). For example, the Hetao Plateau takes about 5 billion m³ water every year from the Yellow River. The annual gross water use of the Yellow River Basin shows a gradual increase from the 1950s to the 2000s. Although industry water use has been increasing since the early 2000s due to the economic development, irrigation remains to be the most important mode of water use in this area. However, most studies on the Yellow River did not explicitly consider river water use in large-scale irrigation districts.

Several previous studies (Jia et al., 2006; Cong et al., 2009; Yuan et al., 2016; Liu et al., 2011; Yin et al., 2021) have applied physically based hydrological models to study the water resources in the Yellow River Basin. Some of these earlier studies (e.g. Cong et al., 2009; Yuan et al., 2016) only simulated natural streamflows and the hydrological models used were calibrated and evaluated against naturalized streamflow observation plus water use data from the regional census. To the best of our knowledge, Yuan et al. (2016) applied an experimental seasonal hydrological forecasting system, which integrated the variable infiltration capacity (VIC, Liang et al., 1996) land surface hydrological model and a global routing model (Yuan et al., 2015a) using an automatic calibration procedure with the shuffled complex evolution (SCE) algorithm (Duan et al., 1994), and obtained the best model performance with the highest Nash–Sutcliffe efficiency (NSE) compared to other studies. Furthermore, some other studies have already simulated real streamflow and considered the impact of water use and other human activities (e.g., damming). Two of these are most important and advanced. Jia et al. (2006) developed the WEP-L distributed hydrological model which combines a hydrological model with a water use module using census irrigation data as input, to assess the water resources in the Yellow River Basin. Yin et al. (2021) applied a global land surface model ORCHIDEE (ORganizing Carbon and Hydrology in Dynamic EcosystEms) and integrated new irrigation and crop module and an offline dam operation model to improve the model performance. However, Jia et al. (2006) implemented census irrigation data as input to the model, and the irrigation water requirements depended on statistical methods and data rather than being based on physical laws. Yin et al. (2021) did not consider long-distance water transfer and assumed that streams only supply water to the crops within the grid cells they across, according to the ORCHIDEE river routing scheme. This limitation may lead to an underestimation of irrigation water requirements which depend on grid size and causes problems for simulating the hydrological processes over large irrigated districts.

The main purpose of this article is to improve the performance of long-term and large-scale hydrological simulation over the Yellow River Basin using the offline mode of the coupled Atmospheric and Hydrological Modelling System (AHMS) being developed at the University of Cologne (Xia, 2019). As river water use for irrigation in semi-arid and arid regions, such as the large irrigation districts in the Yellow River Basin, profoundly impacts on the hydrological processes, we extend the AHMS to include river water use process to better simulate the streamflow and assess the water resource in the Yellow River Basin. To this end, the channel routing model is extended to account for river water use for irrigation, and irrigated water requirements estimated by the WATNEEDS model (Chiarelli et al., 2020) is used as the input to the channel routing model. As we will show in the subsequent sections, our contribution leads to improved offline AHMS simulations, by reducing the errors associated with the underestimation of evaporation and the overestimation of runoff. Furthermore, we show that the modelling of streamflow in the arid and semi-arid regions of the Yellow River Basin improves upon consideration of irrigation.

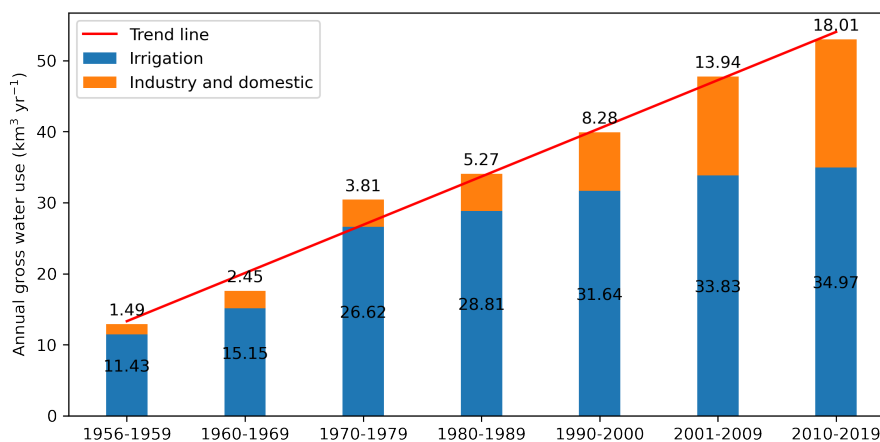


Figure 1: Annual gross water use in Yellow River Basin from 1956 to 2019 (for the period 1956 to 2000 data were obtained from Jia et al. (2006); for the period 2001-2019 data were collected from Yellow River Bulletin of Water Resources wrote by the Yellow River Conservancy Commission (YRCC) of the Ministry of Water Resources of China (<http://www.yrcc.gov.cn/other/hhgb/>)).

2. Method

2.1. The offline mode of the coupled Atmospheric and Hydrological Modelling System

The Atmospheric and Hydrological Modelling System (AHMS) is a fully coupled atmospheric and hydrological modelling system (Xia, 2019), which integrates an atmospheric model WRF (Skamarock and Klemp, 2008) and a physically-based distributed regional hydrological model HMS (Yu et al., 2006) through a land surface model NoahMP-LSM (Chen and Dudhia, 2001; Niu et al., 2011). The coupling method developed in WRF-Hydro (Gochis et al., 2013) for downscaling and upscaling of variables between land surface model and hydrological model grids is adopted. The AHMS can either be run offline by using prescribed near-surface atmospheric forcing variables or coupled with the WRF model. A schematic illustration of the online and offline AHMS versions is shown in Fig. 2. The near-surface atmospheric forcing data required to run the AHMS offline includes incoming shortwave and longwave radiation, specific humidity, precipitation, air temperature, surface pressure, and near-surface wind (Table 4).

The following subsections provide a summary of the main components of the AHMS. The simplified sketch of the hydrologic cycle represented in the AHMS is shown in Fig. 3. As illustrated, the channel routing model is extended to account for river water use for irrigation in this study.

2.2. Land surface model

The land surface model NoahMP is a single-column model that simulates atmosphere and land surface exchanges of heat, moisture and momentum. It provides a multi parameterization framework that allows its applications with different combinations of schemes for land surface processes (Chen and Dudhia, 2001; Niu et al., 2011). The NoahMP physics options and parameter tables used in this study are listed in Tables 1 and 2. Only hydrological component infiltration capacity related to the runoff generation scheme is described below. More details about heat, soil moisture, vegetation schemes of NoahMP are described in Chen and Dudhia (2001) and Niu et al. (2011).

2.2.1. Infiltration capacity

Infiltration capacity or maximum infiltration rate is a variable that determines the generation of infiltration excess (Horton) runoff. The infiltration capacity should be represented as the actual soil hydraulic conductivity of the topsoil layer, which is a variable maximum infiltration rate (VIC) depending on the properties of the soil, such as soil moisture and texture. However, the infiltration capacity is also affected by many other factors, such as the heterogeneity of rainfall, topography, even surface organic matter, soil crust and rock in sub-grid at the land surface. Largeron et al. (2018) have found that the soil hydraulic conductivity of the top layer in the soil model is able to represent maximum infiltration rate only when the model is applied in the intense rainfall, while maximum infiltration rates are greatly

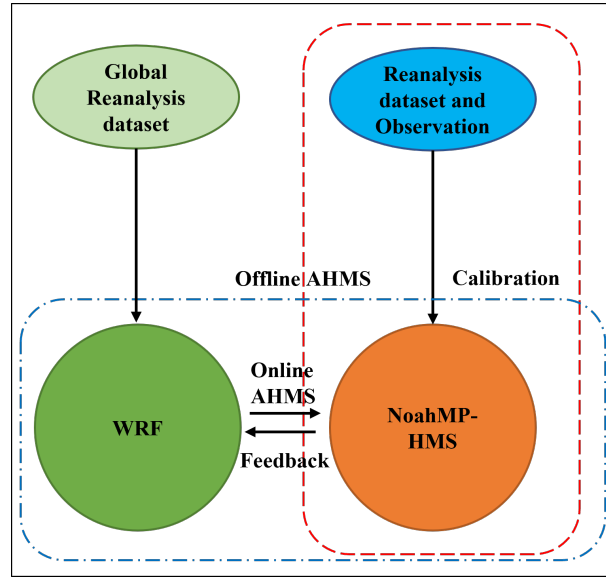


Figure 2: Simplified schematic of the online AHMS (frame with blue dot-dashed line) and offline AHMS (frame with red dashed line). Modified after Wagner et al. (2016b).

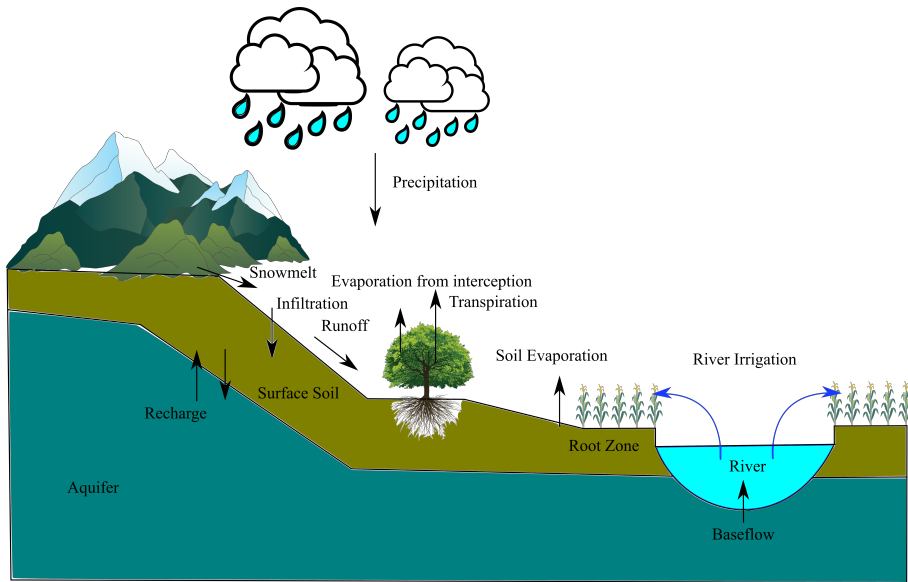


Figure 3: Sketch of the hydrologic cycle as represented in the AHMS.

underestimated in the semi-arid and arid area with low precipitation. Here, the infiltration capacity I_{max} depends on the soil saturated hydraulic conductivity K_{sat} , as shown below.

$$I_{max} = \beta K_{sat} \quad (1)$$

where β is a decay factor, which can be determined by calibration of the annual average runoff in sub-basins.

2.3. Hydrological model

The hydrological model (HMS) is initially developed for mesoscale and large-scale hydrological simulation by Yu et al. (2006), but has been substantially improved in the recent development at the University of Cologne. The

Table 1
Noah-MP parameterization options used in this study

Parameterizations Description	Schemes Used
Dynamic vegetation	4: table LAI, shdfac = maximum
Stomatal resistance	1: Ball-berry, related to photosynthesis (Ball et al., 1987)
Soil moisture factor controlling stomatal resistance	1: Noah scheme, function of moisture (Chen and Dudhia, 2001)
Runoff and groundwater	9: Darcy's law (Xia, 2019)
Surface exchange coefficient for heat	1: M-O (Brutsaert, 2013)
Supercooled liquid water in frozen soil	NY06 (Niu and Yang, 2006)
Frozen soil permeability	1: NY06 (Niu and Yang, 2006)
Radiation transfer	3: gap = 1—FVEG
Snow surface albedo	2: CLASS (Verseghy, 1991)
Partitioning precipitation into rainfall and snowfall	1: Jordan91 (Jordan, 1991)
Lower boundary condition of soil temperature	1: zero flux
The first-layer snow or soil temperature time scheme	1: semi-implicit

Table 2
Parameter tables for the Noah-MP land surface model (Gochis et al., 2020)

Filename	Description
GENPARAM.TBL	Miscellaneous model parameters that are applied globally
MPTABLE.TBL	Vegetation parameters indexes by land use/land cover categories
SOILPARAM.TBL	Soil parameters indexed by soil texture classes

HMS can explicitly simulate the complete hydrological process, including surface water flow, groundwater flow and interactions between them. It consists of three sub-models: a two-dimensional terrestrial hydrological model (RT2D), a two-dimensional ground-water hydrological model (GW2D) and a groundwater and channel interaction model (GCI). Streamflow, groundwater flow from cell to cell and exchange with the stream are estimated in the above modules, respectively. The definitions and formulas of the most important variables and parameters of the HMS are summarized below.

2.3.1. 2D groundwater model

The dynamics of unconfined groundwater is described by the following partial differential Boussinesq equation.

$$S_s \frac{\partial h_g}{\partial t} = \frac{\partial}{\partial x} \left(K_x \frac{\partial h_g}{\partial x} \right) + \frac{\partial}{\partial y} \left(K_y \frac{\partial h_g}{\partial y} \right) + \frac{\partial}{\partial z} \left(K_z \frac{\partial h_g}{\partial z} \right) - Q_{net} \quad (2)$$

where K_x , K_y , K_z are the along-stream, cross-stream and vertical components of the saturated hydraulic conductivity [m s^{-1}], respectively, h_g is groundwater head [m], S_s is the specific storage of porous material [m^{-1}], Q_{net} is the sink and source term, e.g., interaction of groundwater and unsaturated soil, exchange of rivers and groundwater, extraction of groundwater from wells [s^{-1}].

2.3.2. Channel routing model

River and lake levels are represented by one prognostic variable h_r , the thickness of surface water averaged over the grid cell. By combining the continuity of mass in the cell and the momentum equation between cells for transport, the rate of change of h_r is given by

$$A \frac{\partial h_r}{\partial t} = \frac{\partial}{\partial x} \left(A_c \frac{1}{n} R^{2/3} \left| \frac{\partial h_r}{\partial x} \right|^{-1/2} \frac{\partial h_r}{\partial x} \right) + \frac{\partial}{\partial y} \left(A_c \frac{1}{n} R^{2/3} \left| \frac{\partial h_r}{\partial y} \right|^{-1/2} \frac{\partial h_r}{\partial y} \right) + R_t - f_w(C_g + C_u) - C_l - Q_{irr} \quad (3)$$

where h_r is the depth of stream [m], t is time [s], A is the river bed area of water in the river or lake [m], A_c is the cross-sectional area of water in the river or lake at cell boundaries [m], R is the hydraulic radius [m], which is equivalent to $wd/(2d + w)$ for an open channel flow through a rectangular cross section, w and d are the width and the depth of the river [m], respectively, n is Manning's Roughness coefficient [$s\ m^{-1/3}$], note that the x -direction and y -direction average streamflow represents all eight directions between the cells including the diagonal (for clarity, omit it in this formula), R_t is the surface runoff [$m^3\ s^{-1}$] which includes infiltration-excess runoff (R_{ins}) and saturation-excess runoff (R_{sat}), f_w is the wetted surface fraction, set to f_b for running rivers, or to 1 for lakes, C_g is water exchange flux between saturated soil and river [$m^3\ s^{-1}$], C_u is water exchange flux between unsaturated soil and river [$m^3\ s^{-1}$], C_l is water exchange flux between lake and river [$m^3\ s^{-1}$] and Q_{irr} is the water use for irrigation, which has been added to the model in this study [$m^3\ s^{-1}$]. Q_{irr} is equal to the irrigated water requirements of the main channel cross grid and adjacent grids, according to the river routing scheme of the AHMS.

The Manning equation is used to estimate the average velocity $V_{x,y}$ [$m\ s^{-1}$] of the river flow cross-section. It is defined through the expression

$$V_{x,y} = n^{-1} R^{2/3} S_f^{1/2} \quad (4)$$

where n is the Manning roughness coefficient [$s\ m^{-1/3}$], R is the hydraulic radius [m] and S_f is the friction slope [-]. To model $V_{x,y}$, we apply the diffusive wave equation by neglecting the local and convective acceleration terms and assuming that $S_f = S$, where S is the water surface slope [-]. Here, we follow Chow (2010); Yamazaki et al. (2011); De Paiva et al. (2013) and consider that the Manning roughness coefficient is independent of the position throughout the Yellow River Basin. The sensitivity of the AHMS to the Manning roughness coefficient n is discussed in Section 3.5.

2.3.3. Interaction fluxes of river-groundwater and river-vadose

In the land surface model, the subsurface runoff (R_b) is usually formulated as the gravitational free drainage at the bottom of the model (Noah) or parameterized as a function of the groundwater level (NoahMP and CLM). In this study, because of the given river channel in HMS, the subsurface runoff can be explicitly calculated by applying Darcy's equation for the groundwater table and the height of the water level in the river. The river-groundwater (C_g) and river-vadose (C_u) interaction fluxes are calculated using Darcy's law (Yu et al., 2006; Sophocleous, 2002). It is assumed that there is a layer of low-permeability material at the riverbed so that the water in the river can be separated from the groundwater system in each grid. If the water table is higher than the river bed, then C_g is proportional to $h_r - h_g$, and $C_u=0$, where h_r is the elevation of water level in the river and h_g is the groundwater. If groundwater table is lower than river bed, then C_u is proportional to $h_r - h_{bot}$, and $C_g=0$, where h_{bot} is the elevation of stream bed. As described above, the exchange flow between river and groundwater is calculated by the following formula:

$$C_g = \frac{K_b}{M} (h_r - h_g) = C_s (h_r - h_g) \quad (5)$$

$$C_u = C_s (h_r - h_{bot}) \quad (6)$$

where C_s is the hydraulic conductance of stream-aquifer interconnection [s^{-1}], K_b is the hydraulic conductivity of streambed material [$m\ s^{-1}$], M is the streambed thickness [m], h_r is the elevation of water level in the stream [m], h_g is the groundwater head [m], h_{bot} is the elevation of the streambed [m]. The hydraulic conductance of the river bed usually needs to be calibrated against the observed base flow of the river. The sensitivity of AHMS to C_s is discussed in Section 3.5.

2.3.4. Width and depth of Channel

The hydraulic geometric relationship of the channel is in the form of the power-law function of the bankfull discharge Q_{BF} as (Leopold and Maddock, 1953)

$$\begin{aligned} w &= a Q_{BF}^b \\ d &= c Q_{BF}^f \end{aligned} \quad (7)$$

where w and d are the width and the depth of the river, respectively, and Q_{BF} is the bank full discharge [$\text{m}^3 \text{s}^{-1}$], which is estimated by multiplying the upstream area by uniform local river input (assumed is that the local river input is 0.5 mm/day based on the average of historical data) for each cell (Yu et al., 2006). Furthermore, a and c are empirical coefficients, while the exponents b and f are found to vary in different river systems (Leopold and Maddock, 1953), but b has a value around 0.5. In the Yellow River Basin, empirical coefficients such as a and c are estimated from measurement data (Google Earth). Since the river routing model needs to define the width and depth of the channel in each grid, we assume that the minimum values of depth and width are 2 m and 10 m, respectively. The sensitivity of the AHMS to river geometry (width and depth) is discussed in Section 3.5. The width and depth of the river are defined as follows

$$\begin{cases} w = \max[10 * Q_{BF}^{0.5}, 10.0] \\ d = \max[0.6 * Q_{BF}^{0.3}, 2.0] \end{cases} \quad (8)$$

2.3.5. The fractional area of the river bed

Flood inundation is simulated using a simple storage model (Cunge, 1980; De Paiva et al., 2013), assuming that (1) the flow velocity parallel to river direction vanishes on the floodplain, (2) the floodplain acts only as storage areas and (3) water level of the floodplain equals the water level of the main channel. As is shown in Fig. 4, the fractional area of the river bed f_b is estimated as

$$f_b = \left(\frac{w}{dx}\right)^\alpha \quad (9)$$

where w is the width of the channel [m] and dx is the grid size [m]. The default value of α is 0.5, which is in general related to the river's meandering and floodplain geometry. The sensitivity of AHMS to floodplain geometry is discussed in Section 3.5.

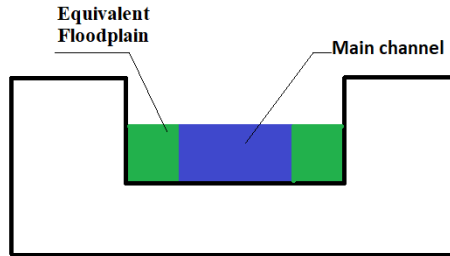


Figure 4: Simple river-floodplain storage model used in the sub-grid cross-section of the AHMS. The main channel area (blue) corresponds to the parameter A_c in Eq. (3). Furthermore, the equivalent floodplain area (green) based on the f_b of Eq. (9). Modified after Cunge (1980).

2.4. Terrestrial water budget and changes

The discharge and balance of water play a key role in the water cycle, so quantifying and assessing budget and changes of terrestrial water storage is essential. The total terrestrial water storage S_t and the terrestrial water balance are given below

$$S_t = W_{sn} + W_{un} + W_{sf} + W_{gw} \quad (10)$$

$$\Delta S_t = \Delta W_{sn} + \Delta W_{un} + \Delta W_{sf} + \Delta W_{gw} \quad (11)$$

$$\frac{dS_t}{dt} = P - ET - R_{sf} - R_{sub} \quad (12)$$

Table 3

Information of four major reservoirs along the mainstream of Yellow River

Reservoirs	Location	Height (m)	Storage (10^9 m ³)	Time of completion
Sanmenxia	Middle reaches	335	9.7	September 1960
Liujiaxia	Upper reaches	147	5.7	October 1968
Longyangxia	Upper reaches	178	27.6	October 1986
Xiaolangdi	Middle reaches	160	12.7	October 1999

where S_t is total terrestrial water storage [m], W_{sn} is the water storage in snowpack (liquid equivalent) [m], W_{un} is the soil moisture storage in unsaturated soil layer [m], W_{sf} is the surface water storage [m], including water storage in the rivers, lakes and reservoirs, W_{gw} is the groundwater water storage [m], P is the precipitation [$m\ s^{-1}$], ET is the evapotranspiration [$m\ s^{-1}$], R_{sf} is the surface runoff [$m\ s^{-1}$], including infiltration-excess runoff and saturation excess runoff, R_{sub} is the subsurface runoff [$m\ s^{-1}$], including the interaction fluxes of river-groundwater C_g and river-vadose C_u .

3. Application to the Yellow River Basin

3.1. Study area

The Yellow River flows across Qinghai-Tibet Plateau, Inner Mongolia Plateau, Chinese Loess Plateau and Huanghuaihai Plain. Most areas on the Chinese Loess Plateau are arid and semi-arid regions. The Yellow River Basin is as shown in Fig 5. The basin has a mean annual air temperature of -4° and annual precipitation of about 450 mm, which is unevenly distributed. This region is characterized by plateau and temperate climate and is strongly affected by the East Asian monsoon. The area of the upper and middle reaches above the Huayuankou station is 730,036 km², thus accounting for 91.82% of the total basin area. The mean annual runoff at the Huayuankou station is 56.7 billion, which corresponds to 96.42% of the total runoff of the Yellow River. The Yellow River area located below the Huayuankou station is an above-ground hanging river with a small catchment area, which covers about 3% of the Yellow River Basin(excluding the internal flow area of 42,000 km²). Therefore, this study focuses on the upper reaches of the Huayuankou station, and the part of the Yellow River Basin referred to in this study corresponds to the upper reaches of the Huayuankou. Furthermore, these upper reaches of Huayuankou station are divided into four subbasins, namely TNH, TNH-LZ, LZ-TDG and TDG-HYK, which are associated with the four key hydrological stations in the region – including Tangnaihe, Lanzhou, Toudaoguai and Huayuankou.

Human activities, such as irrigation mentioned in Section 1 and dam regulation, significantly affect the Yellow River Basin. Table 3 shows the information of the four most influential constructed reservoirs along the mainstream of the Yellow River. Figure 6 shows the annual cycle of the Longyangxia and Sanmenxia Reservoir inflow and outflow. This figure indicates that streamflow at the Longyangxia Reservoir decreased in summer and increased streamflow in autumn during the period from 1979 to 1988. The Sanmenxia Reservoirs increased the baseflow in spring for water supply to the downstream agricultural irrigation areas.

3.2. Model input data

A Lambert conformal projection with standard parallel 38.3° N centered at 109.0° E is used to process input data at a resolution of 20 km for the Yellow River Basin.

3.2.1. Topography data

The high-resolution geographic digital elevation data set HYDRO1k from U.S. Geological Survey with 1-km resolution is used and upscaled to 20-km resolution by using a AHMS pre-processing program (Yu et al., 2006). In the upscaling process, the lower values are weighted more strongly to derive a consistent river network (Yang et al., 2007). The AHMS pre-processing program and ArcSWAT are combined to obtain the related hydrological data, e.g., river depth and width, water surface elevation, upstream area and sub-basin area. As mentioned before, the depth and width of the river channel are estimated from the empirical channel discharge-depth-width relationship based on the theory of hydraulic geometry (Leopold and Maddock, 1953; Neal et al., 2012).

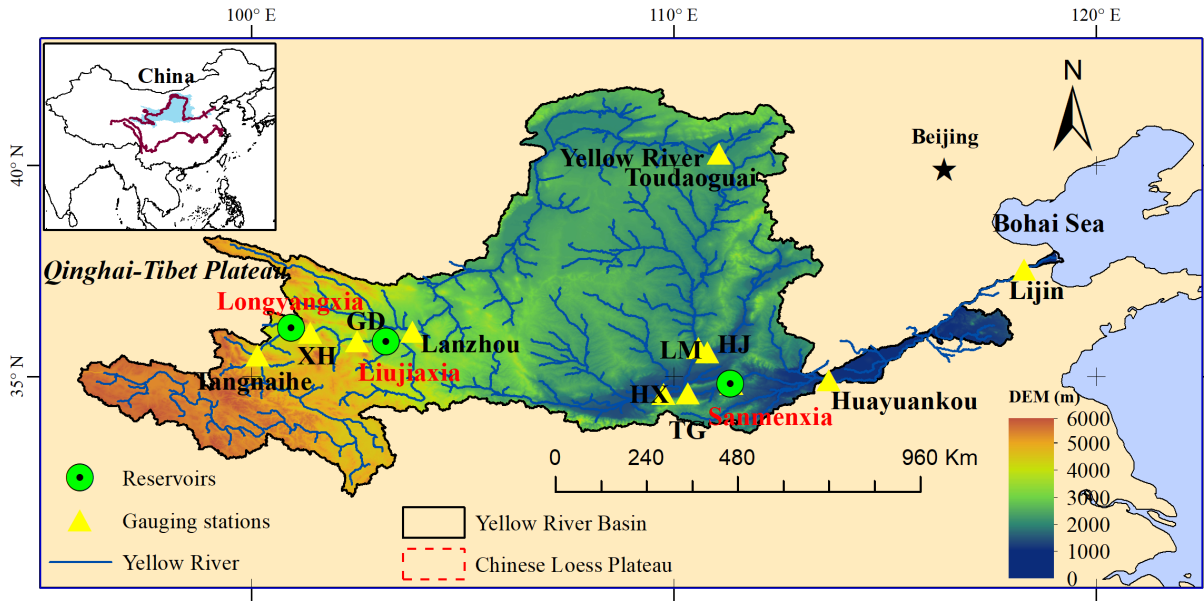


Figure 5: Location and topography of the Yellow River Basin. The map includes the Chinese Loess Plateau, the river network and the four main hydrological stations referred to in the main text, i.e., Tangnaihe (TNH), Lanzhou (LZ), Toudaoguai (TDG) and Huayuankou (HYK). The yellow triangles indicate both these main stations, as well as the stations of Guide (GD), Longmen (LM), Huaxian (HX) and Hejin (HJ), considered to evaluating the impacts of reservoirs on streamflow. The main reservoirs are indicated by the green cycles in the figure.

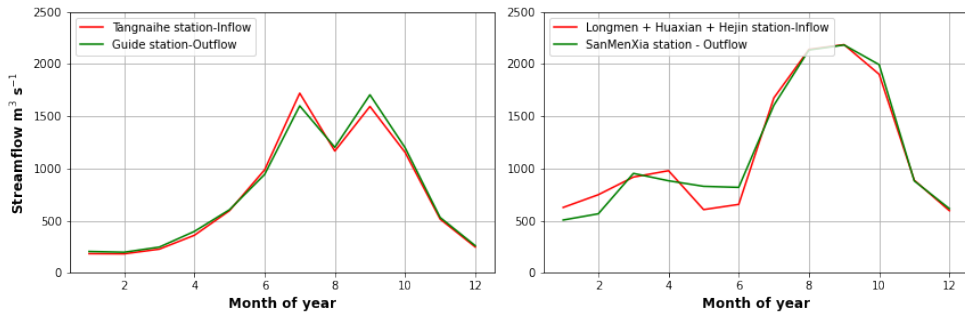


Figure 6: Annual cycles of measured monthly inflow (Tangnaihe station) and outflow (Guide station) of the Longyangxia reservoir and monthly inflow (Longmen plus Haxian and Hejin station) and outflow (Sanmenxia station) of the Sanmenxia reservoir, averaged over 1979-1988.

3.2.2. Subsurface data

The initial groundwater head is derived from the simulations using the global groundwater model (de Graaf et al., 2015). Based on the China 1:4 000 000 Geology Dataset, the hydrogeologic parameters, such as aquifer thickness, porosity and hydraulic conductivity of the aquifer are obtained correspondingly for each lithologic type with a lookup method (Yang et al., 2010).

3.2.3. Meteorological data

The forcing data applied in our simulations is obtained from the China Meteorological Forcing Dataset (CMFD) (He et al., 2020). These data include precipitation, near-surface air temperature, near-surface specific humidity, surface pressure, near-surface wind, surface downwelling shortwave and longwave radiation, as specified in Table 4. CMFD is a high spatial-temporal resolution gridded near-surface meteorological dataset, which is especially designed for studies of land surface processes in China. This dataset was generated by combining remote sensing products, reanalysis datasets

Table 4

List of input initial and boundary conditions associated with meteorological forcing, topography, soil and vegetation and hydrology to run the AHMS in offline mode.

Name	Description	Unit	Source
<i>Meteorological forcing</i>			
Wind	Near-surface wind speed	$m\ s^{-1}$	CMFD Reanalysis products
Tair	Near-surface air temperature	K	
PSurf	Surface air pressure	$N\ m^{-2}$	
Qair	Near-surface specific humidity	$kg\ kg^{-1}$	
LWdown	Surface downwelling longwave radiation	$W\ m^{-2}$	
SWdown	Surface downwelling shortwave radiation	$W\ m^{-2}$	
Rainf	Rainfall flux	$kg\ m^{-2}\ s^{-1}$	
Snowf	Snowfall flux	$kg\ m^{-2}\ s^{-1}$	
<i>Topograph, Soil and Vegetation</i>			
H_t	Terrain height	m	WRF Geographical database
	Top layer soil type	-	
	Bottom layer soil layer	-	
T	Deep soil temperature	K	
LAI	Monthly leaf area index	-	
f_g	Monthly green fraction	-	
	land use type	-	
α	Monthly suraface albedo	%	
<i>Hydrology</i>			
H_w	hydrological terrain elevation	m	Upscaling of USGS HYDR1K by ZB algorithm
h_0	initial groundwater head	m	Global dataset (de Graaf et al., 2017)
D	unconfined aquifer thickness	m	Chinese geological dataset
B	channel depth and width	m	River hydraulic geometry (Leopold and Maddock, 1953)

and in-situ observations from weather stations. Precipitation fields in CMFD were produced based on the assimilation of 753 weather stations from the China Meteorological Administration (CMA) and gridded background data including TRMM and GLDAS-NOAH.

3.2.4. Irrigated water requirements data from the WATNEEDS model

Chiarelli et al. (2020) published a global gridded database of monthly crop-specific green (rain-fed) and blue (irrigated) water requirements for 23 main crops and 3 crop groups obtained using their WATNEEDS model. The monthly time-step of this global blue (irrigated) water requirements dataset with a 5 arcminute resolution (10 km at the equator) are downloaded from the available repository (<https://doi.org/10.6084/m9.figshare.c.4893084>), and then interpolated to the Yellow River Basin domain model grid in this study.

3.2.5. Validation data

In order to calibrate and validate the AHMS, the observed daily water discharge dataset, publicly available from the National Earth System Science Data Center of the National Science & Technology Infrastructure of China (<http://loess.geodata.cn>) for the period 1979-1988, is adopted, which includes six main gauging stations Tangnaihe (a), Lanzhou (b), Toudaoguai (c) Sanmenxia (d), Huaxian(e) and Huayuankou (f) in the Yellow River Basin. To validate our model prediction for evapotranspiration, we employ the Global Land Evaporation Amsterdam Model (GLEAM) v3.5 Datasets (Martens et al., 2017), which has been developed based on satellite observations. Moreover, Gravity Recovery

and Climate Experiment (GRACE) terrestrial water storage (TWS) data is obtained to evaluate modelled TWS on a regional scale. We downloaded the latest GRACE products of three different analysis centres, (1) the GFZ-RL05 solutions (Dahle et al., 2012) provided by the German Research Centre for Geosciences (GFZ), (2) the CSR-RL05 models (Bettadpur, 2012) calculated by the Center for Space Research (CSR) and (3) the ITG-Grace2010 time-series (Mayer-Guerr et al., 2010) processed at the University of Bonn.

3.3. Model setup and spin-up

The spatial and temporal resolutions of the land surface model and hydrological model are 20 km and 60 minutes. Considering the increasingly intensive human management of the Yellow River in the recent decades, the natural streamflow could have been significantly changed. Therefore, streamflow simulations are performed for the earlier period 1979-1988 for which both observed streamflow and meteorological data are available.

Model spin-up was conducted over decades in the Yellow River Basin to reach dynamic equilibrium form before doing other tests. The vegetation type and soil texture were assumed unchanged for the entire simulation period.

3.4. Model performance evaluation indices

The agreement between the predicted and observed values of a given variable is quantified using the absolute percentage error (*APE*), the coefficient of determination (R^2) and the Nash–Sutcliffe model efficiency coefficient (*NSE*),

$$APE = \left| \frac{O - P}{O} \right| \times 100\% \quad (13)$$

$$R^2 = 1 - \frac{\sum_{i=1}^N (O^i - \bar{O})(P^i - \bar{P})}{\sqrt{\sum_{i=1}^N (O^i - \bar{O})^2} \sqrt{\sum_{i=1}^N (P^i - \bar{P})^2}} \quad (14)$$

where O is the observed value(s), P is the predicted value(s), N is the total number of observations, which are identified by the index i in the summation operator. For streamflow, the corresponding expressions read

$$NSE = 1.0 - \frac{\sum_{i=1}^N (Q_s^i - Q_o^i)^2}{\sum_{i=1}^N (Q_o^i - \bar{Q}_o)^2} \quad (15)$$

where Q_s and Q_o are the predicted and observed values of the streamflow, respectively, and \bar{Q}_o is the mean observed values. *NSE* ranges from minus infinity (poor fit) to 1.0 (perfect fit). In general, model prediction is considered to be satisfactory if $NSE > 0.50$ (Moriasi et al., 2007).

3.5. Parameter calibration and sensitivity analysis

The sensitivity analysis and calibration of hydrological model parameters often require a lot of effort due to large number of the parameters and range of uncertainties. For the land surface model Noah-MP, based on Cuntz et al. (2016), hydrologic output fluxes evapotranspiration and runoff are sensitive to standard and hard-coded parameters related to both soil and vegetation characteristics. However, it is not feasible to consider all sensitive parameters in the land surface model. This paper selects the soil parameters (saturated hydraulic conductivity) that directly affect runoff generation and soil water budget as the most sensitive parameters to calibrate average runoff in the land surface model for further studies. Moreover, the saturated hydraulic conductance of the river bed (C_s) is a calibrated parameter against observed baseflow.

Following Cong et al. (2009), two subbasins were selected to calibrate soil saturated hydraulic conductivity according to the climate, landscape conditions and human activity impact. They are the upstream areas of the

Table 5
Experimental design for parameters sensitivity analysis

Symbol	Name	Unit	Model default	Value
Soil parameters				
β	decay factor of soil saturated hydraulic conductivity	-	calibrated in subbasins as 0.028, 0.035, 0.1 and $0.1 \times K_{sat}$	$\times 0.5, 1.0, 1.5$
C_s	hydraulic conductance of stream-aquifer interconnection	s^{-1}	calibrated in subbasins as $10^{-7}, 10^{-6}, 10^{-6}$ and 10^{-6}	$\times 0.1, 1.0, 10$
River routing parameters				
W	Channel width	m	$10\bar{Q}^{-0.5}$	$\times 0.5, 1.0, 1.5$
B	Channel depth	m	$0.6\bar{Q}^{-0.3}$	$\times 0.5, 1.0, 1.5$
n	Manning roughness coefficient	$s\ m^{-1/3}$	0.025	$\times 0.5, 1.0, 1.5$
α	a exponent used to calculate the fractional of the riverbed	-	0.5	0.4, 0.5, 0.8

Tangnaihai gauge and Wei He Basin (see Fig. 5). The drainage area of Tangnaihe is about 121,972 km². Since there is almost no human activity in this area, the calibrated model parameters can represent the natural hydrological characteristics. The Wei He Basin is the largest subbasin in the middle stream of the Yellow River and the drainage area is approximately 46,827 km². In order to eliminate the influence of human activities in the lower stream of the Tangnaihai gauge, the measured Wei He river streamflow (Hua Xian gauge, see Fig. 5) was used for the calibration of the middle reaches of the Yellow River. As described in Table 5, the calibrated values of soil saturated hydraulic conductivity read $0.028 \times K_{sat}$, $0.035 \times K_{sat}$, $0.1 \times K_{sat}$ and $0.1 \times K_{sat}$ in the subbasins TNH, TNH-LZ, LZ-TDG and TDG-HYK, respectively.

Furthermore, in large-scale hydrological simulations, empirical equations are used to estimate channel parameters due to the lack of a large-scale river hydraulic geometry dataset. In recent years, the use of advanced satellite data has made great progress, thus providing a means to improved quantitative assessment of these parameters. Neal et al. (2012) used high-resolution satellite imagery to estimate the width of rivers, and Yamazaki et al. (2011) developed the Global Width Database of Large Rivers (GWD-LR) based on observed water bodies. However, in hydrological simulations, the width, depth and the Manning roughness coefficient of the channel need to be used in combination, but river depth and the Manning roughness coefficient are still difficult to obtain for the large and data-sparse areas. Based on the previous research on large-scale river dynamics (Yu et al., 2006; Yamazaki et al., 2011; Neal et al., 2012; De Paiva et al., 2013), the Manning roughness coefficient (n), the coefficient of the hydraulic geometry (B and W) and the exponent of river bed fraction (f_b) are selected for sensitivity analysis. The selected model parameters are summarized in Table 5. For example, each parameter of the flow routing model was equally perturbed in the Yellow River Basin by the factors 0.5, 0 and -0.5.

Figure 7 and Figures A1, A2, A3, A4 and A5 in Appendix A display observed annual cycles of averaged weekly streamflow at the main gauging stations along with the associated predictions from our simulations using the different values of β , B , W , n , α and C_s , respectively. As can be seen from these figures, the model results are particularly sensitive to α , β and n . The calibration of the AHMS is thus conducted manually to obtain the optimal combination of the two most sensitive river routing parameters (α and n) and soil parameters (β and C_s) for the upper and middle reaches of the Yellow River. The calibrated hydrographs and the corresponding statistics are presented in Fig. 8. In Fig. 8, the monthly streamflow series predicted with our simulations are compared with the observations at the four gauging stations from 1979 to 1988. The hydrograph is greatly improved by the calibration procedure and a reasonable agreement is found between these observations and the simulation results for upper stream stations (Tangnaihe and Lanzhou). The agreement of the upstream stations is clearly better than other stations in midstream arid region. We thus conclude that the model must be improved to incorporate human activities in the midstream region, such as river irrigation, which is the subject of Section 5.

4. Evaluation and Discussion

The performance of the offline AHMS is evaluated by means of terrestrial water budget analysis and by comparing the predicted and observed mean annual runoff and monthly streamflow, evapotranspiration and terrestrial water storage anomaly in the Yellow River Basin. Moreover, the present section further describes the spatial distribution of

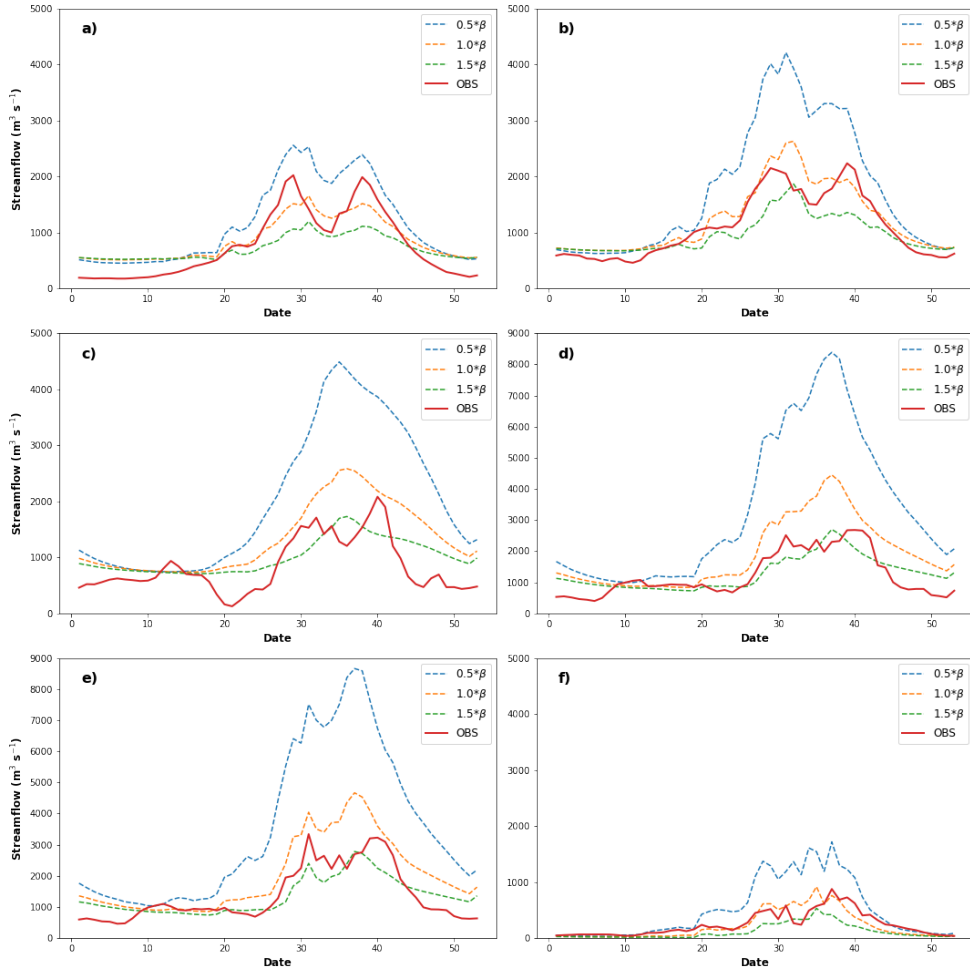


Figure 7: Annual cycles of averaged weekly streamflow for the period of 1979-1988 at six main hydrological stations of the Yellow River, TangnaiHe (a), Lanzhou (b), Toudaoguai (c), Sanmenxia (d), Huayuankou (e) and Huaxian (f), with standard infiltration scheme $\beta * 0.5$ (blue), $\beta * 1.0$ (orange), $\beta * 1.5$ (green) and observed discharge (red), where β is the decay factor of soil saturated hydraulic conductivity. Note the different scales on the Y-axis ($0-5000 \text{ m}^3 \text{ s}^{-1}$ for subfigures a, b, c and f; $0-9000 \text{ m}^3 \text{ s}^{-1}$ for subfigures d and e).

eight hydrological variables including precipitation, evapotranspiration, runoff, streamflow, soil moisture, groundwater depth, surface runoff and subsurface runoff averaged annually from 1979 to 1988.

4.1. Terrestrial Water Budget

Water budget analysis offers a means to verify and evaluate hydrological models (Maurer et al., 2001; De Paiva et al., 2013). We thus perform such an analysis and display the corresponding mean annual terrestrial water budget in Fig. 9. As we can see from this figure, predicted and observed averaged annual precipitation values agree upon an absolute percentage error (APE) of 2%, which gives us confidence that the input precipitation data from CMFD reanalysis products is reliable for the purpose of the present study. The deviation of the model water budget was amounts to about 5% of precipitation and 25% of runoff, while the changes of total terrestrial water storage are about 3% of the precipitation. Furthermore, from the results obtained for the average annual evapotranspiration (APE is 15%) and runoff (APE is 49%), we conclude that the AHMS underestimates the evapotranspiration and overestimates the runoff, if river irrigation is neglected. Based on these findings, we further conclude that irrigation constitutes an essential component of the water balance in the Yellow River Basin, and must be incorporated into the AHMS model to improve the hydrological simulations. In Fig. 10, the mean annual runoff over 1979-1988, as predicted from our

Hydrological Modelling with Irrigation

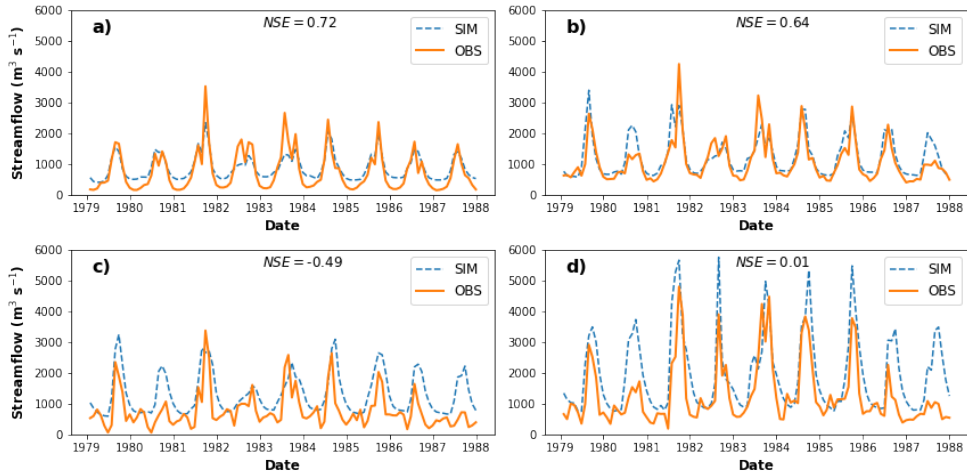


Figure 8: Predicted (blue dashed line) and observed (orange solid line) monthly streamflow from 1979 to 1987 at the hydrological stations: Tangnaihe (a), Lanzhou (b), Toudaoguai (c) and Huayuankou (d).

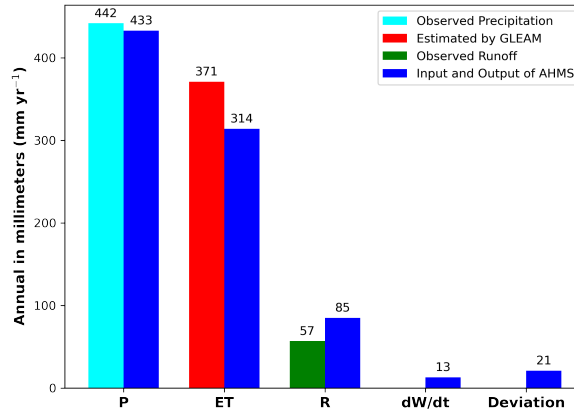


Figure 9: Results from the water budget analysis. Displayed are the predicted and observed annual averaged precipitation, evapotranspiration and runoff over 1979-1988 in the Yellow River Basin. Annual observed precipitation is upscaled from daily precipitation data provided by the China Meteorological Administration, and GLEAM is the Global Land Evaporation Amsterdam Model, while the annual observed runoff is converted from daily streamflow at the gauging station (Huayuankou).

simulations, is compared with the corresponding observation from five gauging stations over the same period, from 1979 to 1988. The APE values of runoff in the subbasins of TNH, TNH-LZ, LZ-TDG, TDG-HYK and Wei He are 3%, 7%, 133%, 49% and 1%, respectively. Therefore, Figure 10 shows that the APE of mean annual runoff is significant at the LZ-TDG subbasin. As mentioned before, the main source of this bias is river water used for irrigation in this region. Therefore, river water used for irrigation is an important component of the water balance, particularly in the semi-arid areas of the Yellow River Basin. Section 5 discusses the incorporation of river water taken for irrigation into AHMS simulations.

4.2. Evapotranspiration

Figure 11 displays monthly evapotranspiration at the Yellow River Basin estimated from the GLEAM, along with the corresponding prediction from the AHMS, for the period from 1980 to 1988. As shown in Fig 11, the AHMS prediction agrees well with the GLEAM estimate, with coefficient of determination $R^2 \approx 0.916$, thus further

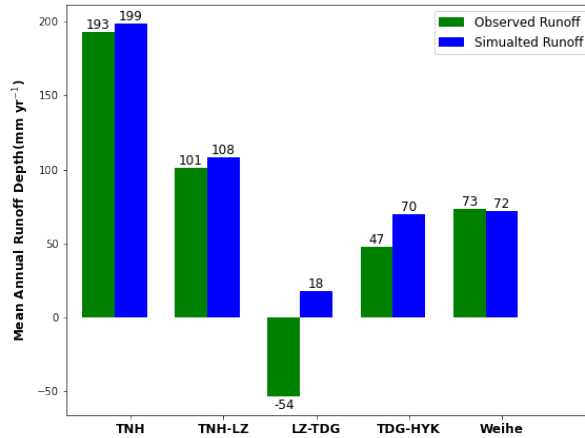


Figure 10: Predicted and observed annual runoff averaged over 1979-1988 in the five subbasins of the Yellow River. Annual observed runoff is converted from the daily streamflow at gauging stations of Tangnaihe, Lanzhou, Toudaoguai, Huayankou and Huaxian.

corroborating the capability of our AHMS simulations to quantitatively describing long-term hydrological processes at the Yellow River Basin.

However, the AHMS underestimates evapotranspiration, especially in winter, notwithstanding the good agreement between the AHMS and GLEAM estimates with regard to the evaporation peaks. In particular, the evapotranspiration in January predicted using AHMS is clearly lower than the corresponding GLEAM estimate. Two factors could explain this underestimation. First, since groundwater provides the main source of water for evaporation during dry seasons, this underestimation of evapotranspiration could be associated with underestimated groundwater recharge in winter. Second, it has been noted in previous studies (Yeh and Famiglietti, 2008; Groisman and Legates, 1994) that measured precipitation from rain gauges have a systematic negative bias because of local winds effect around rain gauges. This negative bias is greater in winter since snowflakes are more prone to wind deflections than raindrops. This underestimation of evapotranspiration may therefore be thus caused by negative bias in precipitation dataset, especially in winter.

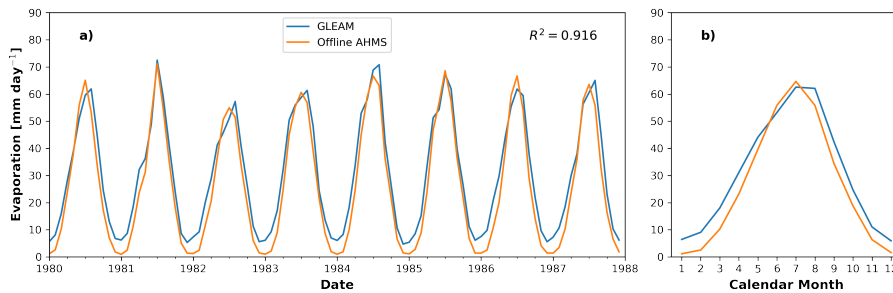


Figure 11: Comparison of evapotranspiration estimated by GLEAM and simulated using AHMS over 1980-1988 for the Yellow River Basin (a) monthly evapotranspiration (b) annual cycles of monthly evapotranspiration.

4.3. Terrestrial Water Storage

The simulated terrestrial water storage anomaly by the AHMS is compared with the GRACE-based results for the entire Yellow River Basin in Fig. 12. We found that the AHMS can better capture the entire water cycle in humid years (2003-2006) and in the winter in dry years (2009-2012), including the time and amplitude of water level fluctuations. It should be noted that the AHMS can only simulate natural TWS anomaly, which does not consider the interference of human activities, such as reservoir storage and agricultural irrigation. For instance, as can be seen in Fig. 12, the

GRACE-based TWS has many small peaks in spring, which may be caused by human irrigation activities, but cannot be observed in the simulation result.

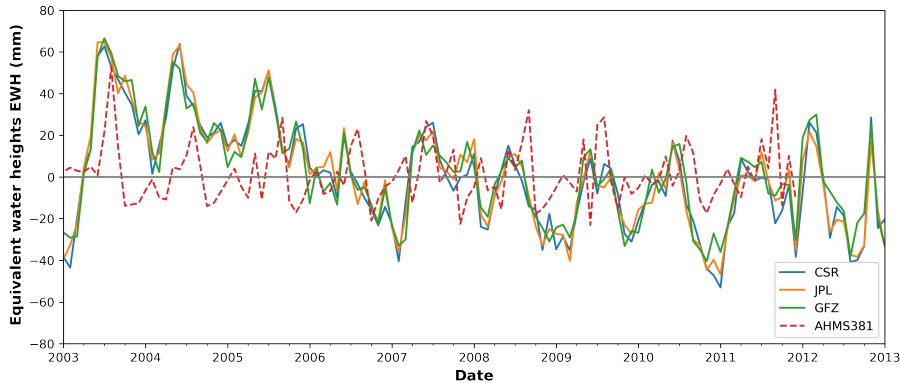


Figure 12: Monthly TWS anomalies over 2003-2012 in the Yellow River Basin calculated from GRACE dataset observation: CSR, JPL, GFZ (solid line) and the offline AHMS simulation (red dashed line)

Figure 13 shows the contribution components of the simulated TWS anomaly, which indicates that soil moisture is the main component of the TWS anomaly, while the groundwater is the second-largest component in the Yellow River Basin. This result is different from the results of De Paiva et al. (2013), who found, by means of MGF-IPH model simulations, that surface water dominates the TWS changes while soil moisture and groundwater constitute the second and third components in the Amazon River Basin, respectively. The partition of the TWS anomaly is consistent with Cai et al. (2014) who simulated the TWS anomaly in the Mississippi River Basin using land surface NoahMP. Through the comparison of the above three regions, we found that for areas with the high precipitation rate (average 2200 mm/yr in Amazon River Basin), the contribution of surface water to the TWS anomaly is the largest, and in areas with a medium and low precipitation rate (average 1000 mm/yr in the Mississippi River Basin and 449 mm /yr in the Yellow River Basin) are governed mainly by soil moisture and groundwater.

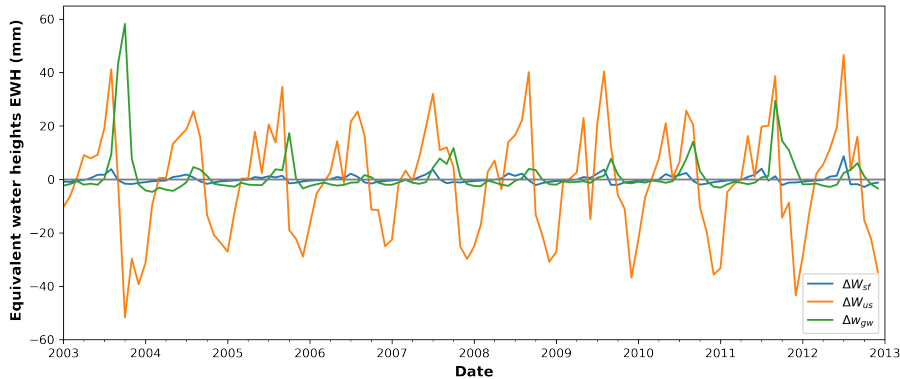


Figure 13: AHMS predictions for the TWS anomalies over 2003-2012 in the Yellow River Basin. Specifically, the figure shows the predicted changes of surface water (ΔW_{sf} ; blue line), soil moisture water (ΔW_{us} ; yellow line), groundwater (ΔW_{gw} ; green line).

4.4. Spatial Distribution of the Hydrological Variables

Figure 14 shows the spatial distribution of hydrological variables including (a) precipitation, (b) evapotranspiration, (c) runoff, (d) streamflow, (e) soil moisture, (f) groundwater depth, (g) surface runoff and (h) subsurface runoff in the Yellow River Basin, averaged annually from 1979 to 1988. As shown in Fig. 14a, the Yellow River Basin has a very uneven distribution of precipitation, decreasing considerably from south (700-1000 mm/yr) to north (100-200 mm/yr).

This distribution of precipitation correlates strongly with the evapotranspiration map (Fig. 14b), and appears consistent with the occurrence of two major runoff areas in the southern part of the Yellow River Basin, i.e., the upper reaches and the Wei He River Basin (Fig. 14c). Furthermore, it can be seen in Fig. 14d that the river network and flow magnitude predicted by the model match the corresponding observations. Figure 14e shows that the maximum and minimum values of soil moisture are in the upper reaches and in the arid to semi-arid middle reaches of Yellow River Basin, respectively, and that soil moisture spatial distribution follows closely the river network. Moreover, groundwater depth exceeds 25 m over most of the Yellow River Basin (Fig. 14f), except for the main river networks and the lower reaches, which have groundwater level under 10 m. Figure 14g shows that the distributions of runoff and surface runoff are consistent with each other, while it can be seen from Fig. 14h that subsurface runoff is mainly generated in the upper reaches, with the Yellow River recharging groundwater from Lanzhou to Toudaoguai.

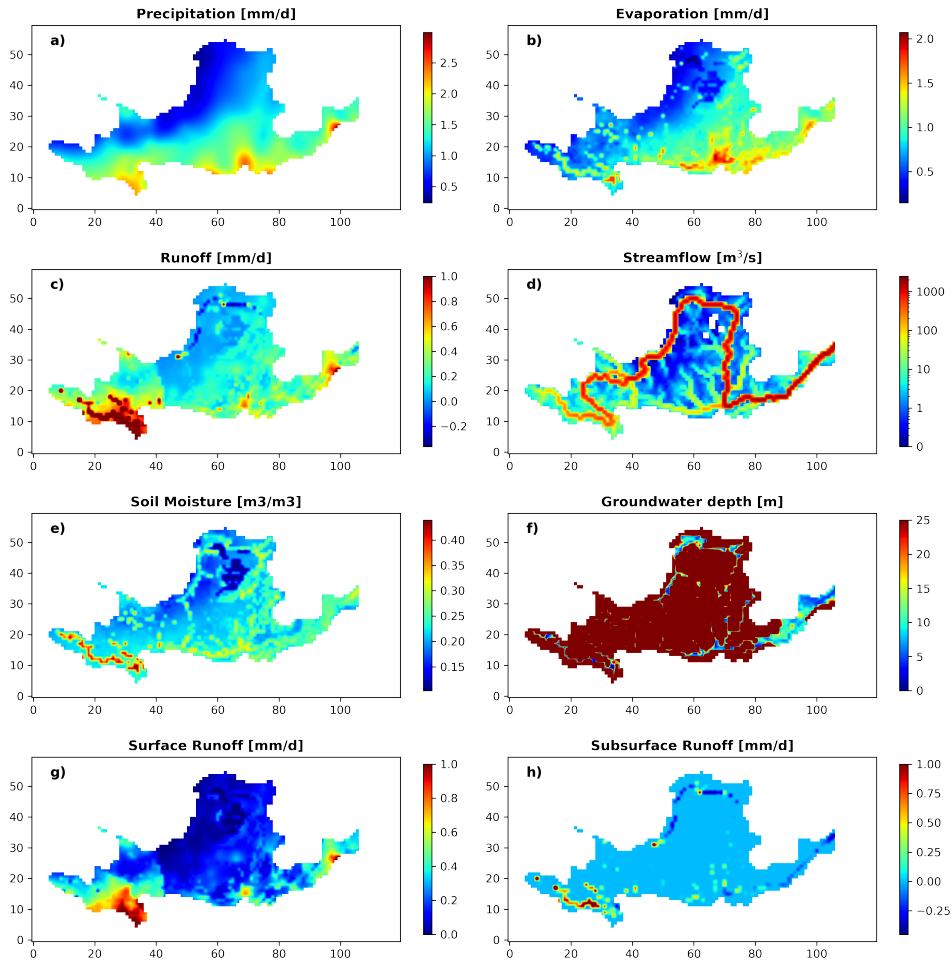


Figure 14: Spatial distributions of the annual mean quantities averaged over 1979-1988 in the Yellow River Basin (a) precipitation, (b) evapotranspiration, (c) runoff, (d) streamflow, (e) soil moisture, (f) groundwater depth, (g) surface runoff, (h) subsurface runoff.

5. Analysis and Simulation of Irrigation Impact on the Runoff, Evapotranspiration and Streamflow

Irrigation water is an important component of water balance in the arid and semi-arid areas and strongly affects streamflow in the Yellow River Basin. As shown in Fig 10, the Lanzhou-Tangnaihe (LZ-TDG) subbasin is a net water

consumption region. However, the operational version of the AHMS did not consider taking water from the Yellow River for irrigation, resulting in a positive average annual runoff in this area.

In this study, the channel routing model of AHMS has been extended for taking water from the river for irrigation (Q_{irr} in Eq. (3)). Specifically, blue (irrigated) water requirements data from the WATNEEDS model (Chiarelli et al., 2020) is used as input data of the irrigation water demand (where and when irrigation has occurred) in the Yellow River Basin, as shown in Fig 15. As seen, the largest and second-largest water use rate is located in the Hetao Plateau and Ning Xia agricultural irrigation districts in the north of the basin. The temporal distribution of irrigation water consumption indicates that the maximum water consumption rate occurs in July. Furthermore, according to the Yellow River Water Resources Bulletin, we neglect the groundwater used for irrigation in this area since the large irrigation districts rely mainly on water abstraction from the Yellow River to meet irrigation water demand. Therefore, we only simulate irrigation taken from the river in the large irrigation districts of LZ-TDG subbasin. Moreover, irrigation water requirements vary from year to year (see Fig. 1) while Chiarelli et al. (2020) estimated the irrigation water demand only for the year 2000. Therefore, the average irrigation water use for the period 1979-1988 in this paper was calibrated by comparing observed and simulated annual runoff in the LZ-TDG subbasin. However, the spatial and temporal distribution of irrigation water requirements are consistent with that of Chiarelli et al. (2020).

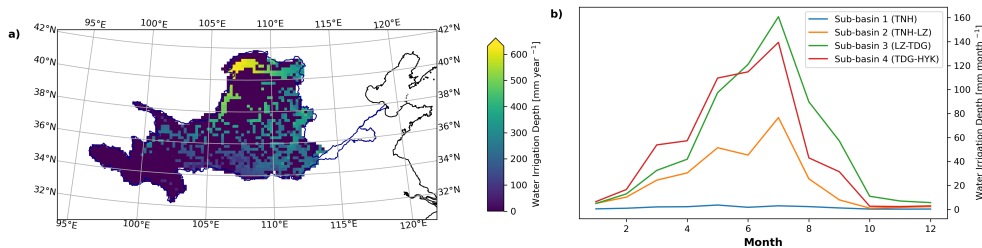


Figure 15: Spatial and temporal distribution of irrigation water requirement over the Yellow River Basin based on the WATNEEDS model dataset (Chiarelli et al., 2020).

Figure 16 displays predicted annual averaged precipitation, evapotranspiration and runoff for the period 1979-1988, obtained from the simulation under consideration of irrigation in the Yellow River Basin, along with the corresponding observations. Compared to the results displayed in Fig. 9 (no irrigation), the absolute percentage error (APE) of evapotranspiration and runoff decreased from 15% to 9% and from 49% to 19%, respectively. Moreover, the annual average runoff obtained from the model with irrigation is compared against the observed value in Fig. 17. As can be seen by comparing Fig. 17 with Fig. 10 (no irrigation), incorporation of irrigation substantially improves the model predictions. In particular, the negative average annual runoff at the LZ-TDG subbasin is accurately reproduced by the model with irrigation, as shown in Fig. 17.

Furthermore, we compare the GLEAM estimate for the evapotranspiration in the Yellow River Basin in the period of 1980-1988 with the corresponding predictions from AHMS simulation, obtained under consideration of taking water from the river for irrigation. The results for the Yellow River Basin are shown in Fig. 18. Since microwave observations of surface soil moisture are assimilated into the GLEAM soil profile to correct for forcing errors in GLEAM (Martens et al., 2016), the evapotranspiration estimated by GLEAM should be able to reflect the effects of irrigation. Indeed, incorporation of irrigation into the model improves considerably the agreement between GLEAM estimates and AHMS predictions of evapotranspiration (Fig. 18), especially in spring, with the coefficient of determination (R^2) increasing from 0.916 to 0.923. However, the AHMS slightly overestimates evapotranspiration in July. A possible explanation for this overestimate may be the lack of a dynamic crop model in our AHMS simulation. However, although different crop models have been considered in previous hydrological simulations (Liu et al., 2016; Wu et al., 2016), further work will be required to develop a reliable crop representation for our AHMS simulations, and to evaluate the role of crop for the model predictions in the Yellow River Basin. This work shall constitute an interesting extension of the model discussed in the present manuscript.

Figure 19 shows the annual cycles of monthly streamflow averaged at the outlet of middle reaches of the Yellow River Basin (Huayuankou station) for 1979-1988, both with and without consideration of taking water from the river for irrigation in the large irrigation districts – including the Hetao Plateau and Ningxia agriculture area. The results displayed in Fig. 19 show that AHMS predictions of streamflow agree more closely with observation data when irrigation is considered in the simulation. Furthermore, consideration of irrigation has led to a reduction in the

Hydrological Modelling with Irrigation

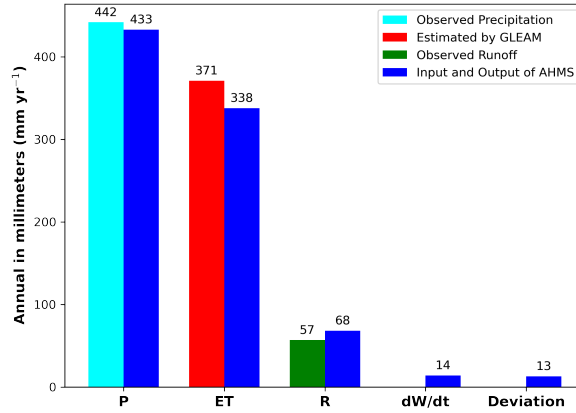


Figure 16: Mean annual terrestrial water budget and comparison of simulated and observed annual averaged precipitation, evapotranspiration and runoff over 1979-1988, for the simulation under consideration of irrigation in the Yellow River Basin.

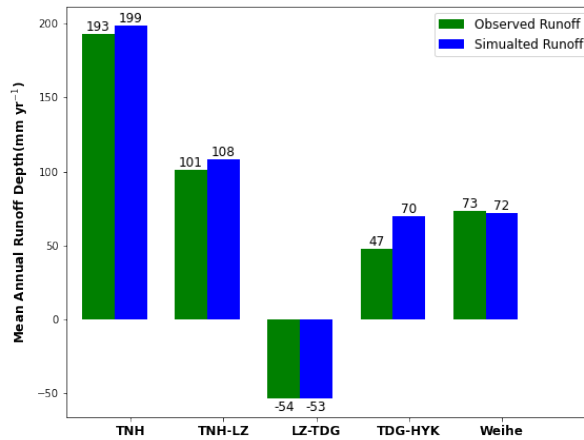


Figure 17: Simulated and observed surface runoff averaged over 1979-1988 in the five subbasins of Yellow River with consideration of taking water from river for irrigation in the Lanzhou to Toudaoguai

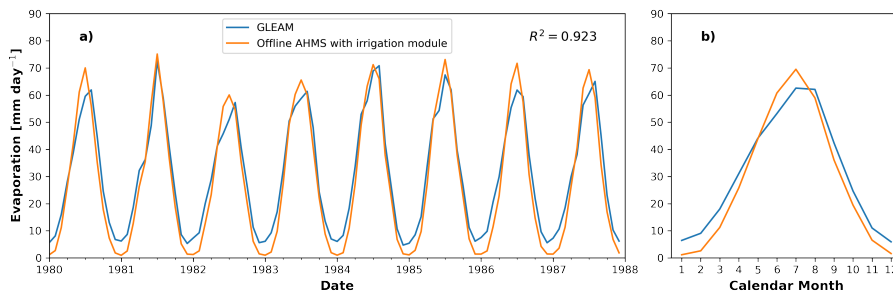


Figure 18: (a) Monthly and (b) annual cycles of monthly evapotranspiration in the Yellow River Basin over 1980-1988, estimated by the GLEAM (blue line) and predicted from the AHMS simulation (orange line) under consideration of taking water from river for irrigation in the Lanzhou to Toudaoguai subbasin.

systematic errors associated with the streamflow simulations. More precisely, the integration error of the streamflow has been reduced from zone *A + B* to zone *B*, with Nash-Sutcliffe model efficiency changing from -0.26 (without

irrigation) to 0.62 (with irrigation). However, various sources for the remaining error associated with the area *B* in Fig. 19 should be elucidated in future work. In particular, these sources include the influence of industrial and domestic water use, as well as dam regulations, not included in our study.

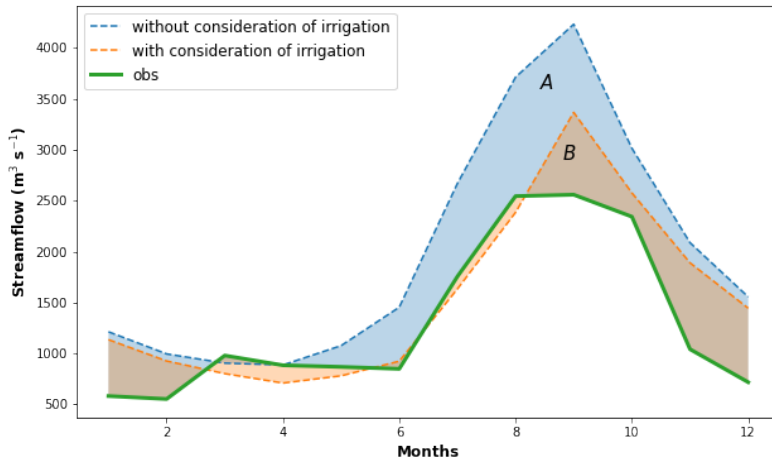


Figure 19: Monthly mean profiles of the annual mean streamflow at outlet of middle reaches of Yellow River Basin (Huayuankou station) for the period of 1978-1988 with and without consideration of taking water from river for irrigation in the LanZhou to TouDaoGuai subbasin.

6. Conclusion

In the present work, the coupled Atmospheric and Hydrological Modelling System (AHMS) has been applied to perform offline hydrological simulations of the Yellow River Basin for the period 1979-2013. AHMS has been calibrated and evaluated for the Yellow River Basin through conducting a parameter sensitivity analysis and a terrestrial water budget analysis, and by comparing model predictions for the mean annual runoff, monthly streamflow, evapotranspiration and terrestrial water storage anomaly with observation data from in-situ and remote sensing datasets.

In order to consider irrigation water consumption in the middle reaches of the Yellow River, the channel routing model has been extended to account for water taken from the river for irrigation. To this end, the irrigated water requirements data from the WATNEEDS model is used as input data of the channel routing model. By incorporating the calibrated and extended river water use module for irrigation into the model, a more realistic hydrologic response in the near outlet of the Yellow River Basin could be obtained.

Quantitative agreement was found between the predicted discharge at the upstream gauging stations, namely, Tangnaihe and Lanzhou, and the corresponding observation data. Furthermore, a reasonable agreement between model TWS anomalies and observations from GRACE could be obtained. Monthly evapotranspiration estimated by GLEAM and the one modeled by AHMS were also found to agree well with each other, with a performance index coefficient of determination (R^2) of 0.9. This good agreement further demonstrates the capability of AHMS for reproducing long-term hydrological processes in the Yellow River Basin.

However, the current version of AHMS needs to be improved in different ways to more accurately representing hydrological processes in the semi-arid and arid areas of the Yellow River Basin. In the present study, only soil parameters were calibrated from the land surface model. The incorporation of vegetation parameters into the calibration of the numerical simulations would constitute one important model extension in future work. Additional measurement data of river and floodplain geometry for the channel routing model of the AHMS would also improve the prediction of timing and peak of the flood. Furthermore, incorporation of anthropogenic influences, such as damming or groundwater supplies for irrigation, and inclusion of a dynamic crop and damming model into AHMS constitute open modelling tasks, which will be important to improve the quantitative assessment of the hydrological processes in future work.

Overall, the calibrated and extended offline AHMS performs well and can better simulate the runoff and streamflow with consideration of irrigated water requirements in the arid and semi-arid region of the Yellow River Basin. The progress achieved in the present work demonstrates the good performance of the AHMS and paves the way for the wider application of AHMS on the regional scale over the Yellow River Basin.

Acknowledgement

This research was supported by the German Research Foundation (DFG) through the Heisenberg Programme "Multiscale Simulation of Earth Surface Processes", project number 434377576. The China Meteorological Forcing Dataset (CMFD) is provided by National Tibetan Plateau Data Center (<http://data.tpdc.ac.cn>). Daily Yellow River discharge data is supported by "Loess Plateau SubCenter, National Earth System Science Data Center, National Science & Technology Infrastructure of China. (<http://loess.geodata.cn>)". The data used in this study can be found online (<https://github.com/JiangCong1990/AHMS-IRRIG>). The authors declare that they have no conflict of interest.

CRedit authorship contribution statement

Cong Jiang: Formal analysis, Methodology, Software, Validation, Writing - Original Draft, Writing - Review & Editing. **Eric J. R. Parteli:** Conceptualization, Supervision, Funding acquisition, Writing - Review & Editing. **Xin Yin:** Investigation, Visualization. **Qian Xia:** Software. **Yaping Shao:** Conceptualization, Supervision, Writing - Review & Editing, Resources.

References

- Abbott, M.B., Bathurst, J.C., Cunge, J.A., O'Connell, P.E., Rasmussen, J., 1986. An introduction to the European Hydrological System—Systeme Hydrologique Europeen, "SHE", 1: History and philosophy of a physically-based, distributed modelling system. *Journal of Hydrology* 87, 45–59.
- Ball, J.T., Woodrow, I.E., Berry, J.A., 1987. A model predicting stomatal conductance and its contribution to the control of photosynthesis under different environmental conditions, in: *Progress in Photosynthesis Research*. Springer, pp. 221–224.
- Bates, P.D., De Roo, A., 2000. A simple raster-based model for flood inundation simulation. *Journal of Hydrology* 236, 54–77.
- Bettadpur, S., 2012. Insights into the Earth System mass variability from CSR-RL05 GRACE gravity fields, in: *EGU General Assembly Conference Abstracts*, p. 6409.
- Beven, K.J., Kirkby, M.J., 1979. A physically based, variable contributing area model of basin hydrology/Un modèle à base physique de zone d'appel variable de l'hydrologie du bassin versant. *Hydrological Sciences Journal* 24, 43–69.
- Brunner, M.I., Slater, L., Tallaksen, L.M., Clark, M., 2021. Challenges in modeling and predicting floods and droughts: A review. *Wiley Interdisciplinary Reviews: Water* 8, e1520.
- Brutsaert, W., 2013. *Evaporation into the atmosphere: theory, history and applications*. volume 1. Springer Science & Business Media.
- Cai, X., Yang, Z.L., David, C.H., Niu, G.Y., Rodell, M., 2014. Hydrological evaluation of the Noah-MP land surface model for the Mississippi River Basin. *Journal of Geophysical Research: Atmospheres* 119, 23–38.
- Chen, F., Dudhia, J., 2001. Coupling an advanced land surface–hydrology model with the Penn State–NCAR MM5 modeling system. Part I: Model implementation and sensitivity. *Monthly Weather Review* 129, 569–585.
- Chiarelli, D.D., Passera, C., Rosa, L., Davis, K.F., D'Odorico, P., Rulli, M.C., 2020. The green and blue crop water requirement WATNEEDS model and its global gridded outputs. *Scientific data* 7, 1–9.
- Chow, V.T., 2010. *Applied Hydrology*. Tata McGraw-Hill Education.
- Collischonn, W., Allasia, D., Da Silva, B.C., Tucci, C.E., 2007. The MGB-IPH model for large-scale rainfall—runoff modelling. *Hydrological Sciences Journal* 52, 878–895.
- Cong, Z., Yang, D., Gao, B., Yang, H., Hu, H., 2009. Hydrological trend analysis in the Yellow River Basin using a distributed hydrological model. *Water Resources Research* 45.
- Cunge, J., 1980. *Practical aspects of computational river hydraulics*. Pitman Publishing Ltd. London,(17 CUN), 1980, 420 .
- Cuntz, M., Mai, J., Samaniego, L., Clark, M., Wulfmeyer, V., Branch, O., Attinger, S., Thober, S., 2016. The impact of standard and hard-coded parameters on the hydrologic fluxes in the Noah-MP land surface model. *Journal of Geophysical Research: Atmospheres* 121, 10–676.
- Dahle, C., Flechtner, F., Gruber, C., König, D., König, R., Michalak, G., Neumayer, K.H., 2012. The new GFZ RL05 GRACE gravity field model time series, in: *Geophys. Res. Abstracts*.
- De Paiva, R.C.D., Buarque, D.C., Collischonn, W., Bonnet, M.P., Frappart, F., Calmant, S., Bulhões Mendes, C.A., 2013. Large-scale hydrologic and hydrodynamic modeling of the Amazon River Basin. *Water Resources Research* 49, 1226–1243.
- Devia, G.K., Ganasri, B.P., Dwarakish, G.S., 2015. A review on hydrological models. *Aquatic Procedia* 4, 1001–1007.
- Duan, Q., Sorooshian, S., Gupta, V.K., 1994. Optimal use of the SCE-UA global optimization method for calibrating watershed models. *Journal of Hydrology* 158, 265–284.
- Gochis, D.J., Barlage, M., Cabell, R., Casali, M., Dugger, A., FitzGerald, K., McAllister, M., McCreight, J., RafieeiNasab, A., Read, L., Sampson, K., Yates, D., Zhang, Y., 2020. The WRF-Hydro modeling system technical description, version 5.1.1. http://www.ral.ucar.edu/projects/wrf_hydro/, 1–107.

- Gochis, D.J., Yu, W., Yates, D.N., 2013. The WRF-Hydro model technical description and user's guide, Version 1.0. http://www.ral.ucar.edu/projects/wrf_hydro/, 1–120.
- de Graaf, I.d., Sutanudjaja, E., Van Beek, L., Bierkens, M., 2015. A high-resolution global-scale groundwater model. *Hydrology and Earth System Sciences* 19, 823–837.
- de Graaf, I.E., van Beek, R.L., Gleeson, T., Moosdorf, N., Schmitz, O., Sutanudjaja, E.H., Bierkens, M.F., 2017. A global-scale two-layer transient groundwater model: Development and application to groundwater depletion. *Advances in Water Resources* 102, 53–67.
- Groisman, P.Y., Legates, D.R., 1994. The accuracy of United States precipitation data. *Bulletin of the American Meteorological Society* 75, 215–228.
- He, J., Yang, K., Tang, W., Lu, H., Qin, J., Chen, Y., Li, X., 2020. The first high-resolution meteorological forcing dataset for land process studies over china. *Scientific Data* 7, 1–11.
- Irannejad, P., Shao, Y., 1998. Description and validation of the atmosphere–land–surface interaction scheme (ALSIS) with HAPEX and Cabauw data. *Global and Planetary Change* 19, 87–114.
- Jia, Y., Wang, H., Zhou, Z., Qiu, Y., Luo, X., Wang, J., Yan, D., Qin, D., 2006. Development of the WEP-L distributed hydrological model and dynamic assessment of water resources in the Yellow River Basin. *Journal of Hydrology* 331, 606–629.
- Jordan, R.E., 1991. A one-dimensional temperature model for a snow cover: Technical documentation for SNTHERM. 89. <http://hdl.handle.net/11681/11677>.
- Julien, P.Y., Saghaian, B., 1991. CASC2D user's manual: a two-dimensional watershed rainfall-runoff model. Ph.D. thesis. Colorado State University. Libraries.
- Largerion, C., Cloke, H., Verhoef, A., Martinez-de la Torre, A., Mueller, A., 2018. Impact of the representation of the infiltration on the river flow during intense rainfall events in JULES. ECMWF Technical Memorandum.
- Leopold, L.B., Maddock, T., 1953. The hydraulic geometry of stream channels and some physiographic implications. volume 252. US Government Printing Office.
- Liang, X., Lettenmaier, D.P., Wood, E.F., Burges, S.J., 1994. A simple hydrologically based model of land surface water and energy fluxes for general circulation models. *Journal of Geophysical Research: Atmospheres* 99, 14415–14428.
- Liang, X., Wood, E.F., Lettenmaier, D.P., 1996. Surface soil moisture parameterization of the VIC-2L model: Evaluation and modification. *Global and Planetary Change* 13, 195–206.
- Liu, L., Liu, Z., Ren, X., Fischer, T., Xu, Y., 2011. Hydrological impacts of climate change in the Yellow River Basin for the 21st century using hydrological model and statistical downscaling model. *Quaternary International* 244, 211–220.
- Liu, X., Chen, F., Barlage, M., Zhou, G., Niyogi, D., 2016. Noah-MP-Crop: Introducing dynamic crop growth in the Noah-MP land surface model. *Journal of Geophysical Research: Atmospheres* 121, 13–953.
- Martens, B., Miralles, D., Lievens, H., Fernández-Prieto, D., Verhoest, N.E., 2016. Improving terrestrial evaporation estimates over continental Australia through assimilation of SMOS soil moisture. *International Journal of Applied Earth Observation and Geoinformation* 48, 146–162.
- Martens, B., Miralles, D.G., Lievens, H., Schalie, R.v.d., De Jeu, R.A., Fernández-Prieto, D., Beck, H.E., Dorigo, W.A., Verhoest, N.E., 2017. GLEAM v3: Satellite-based land evaporation and root-zone soil moisture. *Geoscientific Model Development* 10, 1903–1925.
- Maurer, E.P., O'Donnell, G.M., Lettenmaier, D.P., Roads, J.O., 2001. Evaluation of the land surface water budget in NCEP/NCAR and NCEP/DOE reanalyses using an off-line hydrologic model. *Journal of Geophysical Research: Atmospheres* 106, 17841–17862.
- Maxwell, R.M., Chow, F.K., Kollet, S.J., 2007. The groundwater–land–surface–atmosphere connection: Soil moisture effects on the atmospheric boundary layer in fully-coupled simulations. *Advances in Water Resources* 30, 2447–2466.
- Mayer-Guerr, T., Kurtenbach, E., Eicker, A., 2010. ITG-Grace2010: the new GRACE gravity field release computed in Bonn, in: EGU General Assembly Conference Abstracts, p. 2446.
- Moriasi, D.N., Arnold, J.G., Van Liew, M.W., Bingner, R.L., Harmel, R.D., Veith, T.L., 2007. Model evaluation guidelines for systematic quantification of accuracy in watershed simulations. *Transactions of the ASABE* 50, 885–900.
- Neal, J., Schumann, G., Bates, P., 2012. A subgrid channel model for simulating river hydraulics and floodplain inundation over large and data sparse areas. *Water Resources Research* 48.
- Niu, G.Y., Yang, Z.L., 2006. Effects of frozen soil on snowmelt runoff and soil water storage at a continental scale. *Journal of Hydrometeorology* 7, 937–952.
- Niu, G.Y., Yang, Z.L., Mitchell, K.E., Chen, F., Ek, M.B., Barlage, M., Kumar, A., Manning, K., Niyogi, D., Rosero, E., et al., 2011. The community Noah land surface model with multiparameterization options (Noah-MP): 1. Model description and evaluation with local-scale measurements. *Journal of Geophysical Research: Atmospheres* 116.
- Oleson, K.W., Lawrence, D.M., Gordon, B., Flanner, M.G., Kluzek, E., Peter, J., Levis, S., Swenson, S.C., Thornton, E., Feddema, J., et al., 2010. Technical description of version 4.0 of the Community Land Model (CLM). University Corporation for Atmospheric Research.
- Patro, S., Chatterjee, C., Mohanty, S., Singh, R., Raghuvanshi, N., 2009. Flood inundation modeling using MIKE FLOOD and remote sensing data. *Journal of the Indian Society of Remote Sensing* 37, 107–118.
- Pilgrim, D., Chapman, T., Doran, D., 1988. Problems of rainfall-runoff modelling in arid and semiarid regions. *Hydrological Sciences Journal* 33, 379–400.
- Shrestha, P., Sulis, M., Masbou, M., Kollet, S., Simmer, C., 2014. A scale-consistent terrestrial systems modeling platform based on COSMO, CLM, and ParFlow. *Monthly Weather Review* 142, 3466–3483.
- Skamarock, W.C., Klemp, J.B., 2008. A time-split nonhydrostatic atmospheric model for weather research and forecasting applications. *Journal of Computational Physics* 227, 3465–3485.
- Sophocleous, M., 2002. Interactions between groundwater and surface water: the state of the science. *Hydrogeology Journal* 10, 52–67.
- Tegegne, G., Park, D.K., Kim, Y.O., 2017. Comparison of hydrological models for the assessment of water resources in a data-scarce region, the Upper Blue Nile River Basin. *Journal of Hydrology: Regional Studies* 14, 49–66.
- Verseghy, D.L., 1991. CLASS—A Canadian land surface scheme for GCMs. I. Soil model. *International Journal of Climatology* 11, 111–133.

- Wagner, S., Fersch, B., Yuan, F., Yu, Z., Kunstmann, H., 2016a. Fully coupled atmospheric-hydrological modeling at regional and long-term scales: Development, application, and analysis of WRF-HMS. *Water Resources Research* 52, 3187–3211.
- Wagner, S., Fersch, B., Yuan, F., Yu, Z., Kunstmann, H., 2016b. WRF-HMS, a fully-coupled regional atmospheric-hydrological modeling system for long-term scale applications, in: *EGU General Assembly Conference Abstracts*, pp. EPSC2016–12321.
- Wilby, R., Greenfield, B., Glenny, C., 1994. A coupled synoptic-hydrological model for climate change impact assessment. *Journal of Hydrology* 153, 265–290.
- Wu, X., Vuichard, N., Ciais, P., Viovy, N., Noblet-Ducoudré, N.d., Wang, X., Magliulo, V., Wattenbach, M., Vitale, L., Tommasi, P.D., et al., 2016. ORCHIDEE-CROP (v0), a new process-based agro-land surface model: model description and evaluation over Europe. *Geoscientific Model Development* 9, 857–873.
- Xia, Q., 2019. Development and Application of a Coupled Atmospheric and Hydrological Modelling System. Ph.D. thesis. Universität zu Köln. URL: <https://kups.ub.uni-koeln.de/9450/>.
- Yamazaki, D., Kanae, S., Kim, H., Oki, T., 2011. A physically based description of floodplain inundation dynamics in a global river routing model. *Water Resources Research* 47.
- Yang, C., Lin, Z., Yu, Z., Hao, Z., Liu, S., 2010. Analysis and simulation of human activity impact on streamflow in the Huaihe River Basin with a large-scale hydrologic model. *Journal of Hydrometeorology* 11, 810–821.
- Yang, C., Yu, Z., Lin, Z., Hao, Z., 2007. Method study of constructing digital watershed for large-scale distributed hydrological model. *Progress of Geography* 26, 68–76.
- Yeh, P.J.F., Famiglietti, J., 2008. Regional terrestrial water storage change and evapotranspiration from terrestrial and atmospheric water balance computations. *Journal of Geophysical Research: Atmospheres* 113.
- Yin, Z., Otle, C., Ciais, P., Zhou, F., Wang, X., Jan, P., Dumas, P., Peng, S., Li, L., Zhou, X., et al., 2021. Irrigation, damming, and streamflow fluctuations of the Yellow River. *Hydrology and Earth System Sciences* 25, 1133–1150.
- Yu, Z., Pollard, D., Cheng, L., 2006. On continental-scale hydrologic simulations with a coupled hydrologic model. *Journal of Hydrology* 331, 110–124.
- Yuan, X., Ma, F., Wang, L., Zheng, Z., Ma, Z., Ye, A., Peng, S., 2016. An experimental seasonal hydrological forecasting system over the Yellow River Basin—Part 1: Understanding the role of initial hydrological conditions. *Hydrology and Earth System Sciences* 20, 2437–2451.

A. Sensitivity Analysis

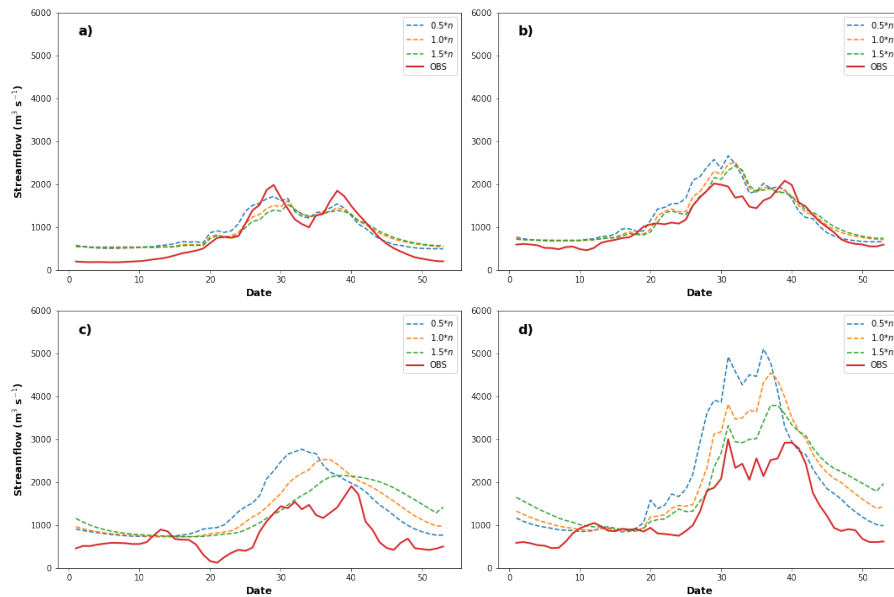


Figure A.1: Annual cycles of averaged weekly streamflow for the period of 1979-1988 at four main stations of Yellow River, Tangnaihe (a), Lanzhou (b), Toudaoguai (c) and Huayuankou (d), with Manning roughness coefficient of river $n \times 0.5$ (blue), n (orange), $n \times 1.5$ (green), observed discharge (red).

Hydrological Modelling with Irrigation

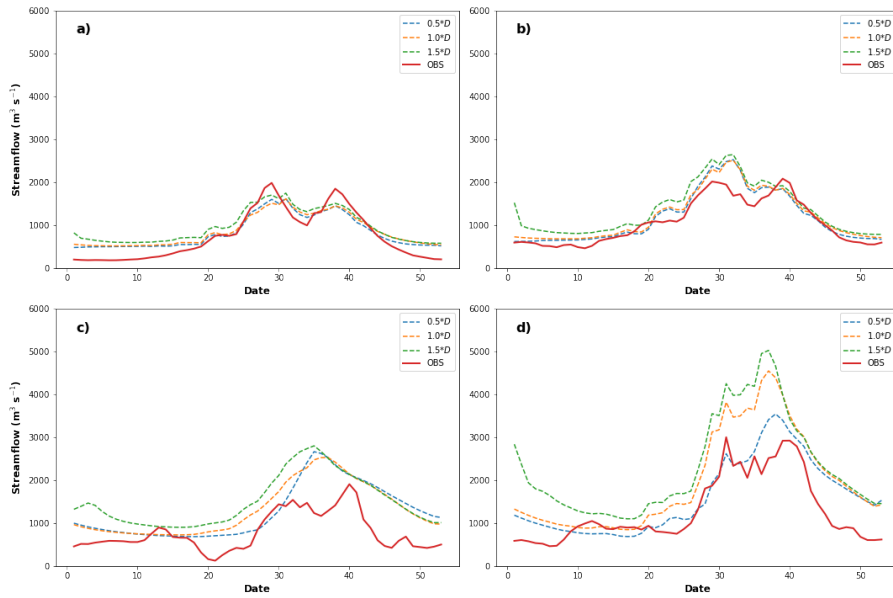


Figure A.2: Annual cycles of averaged weekly streamflow for the period of 1979-1988 at four main stations of the Yellow River, Tangnaihe (a), Lanzhou (b), Toudaoguai (c) and Huayuankou (d), with the depth of river $B \times 0.5$ (blue), B (orange), $B \times 1.5$ (green), observed discharge (red).

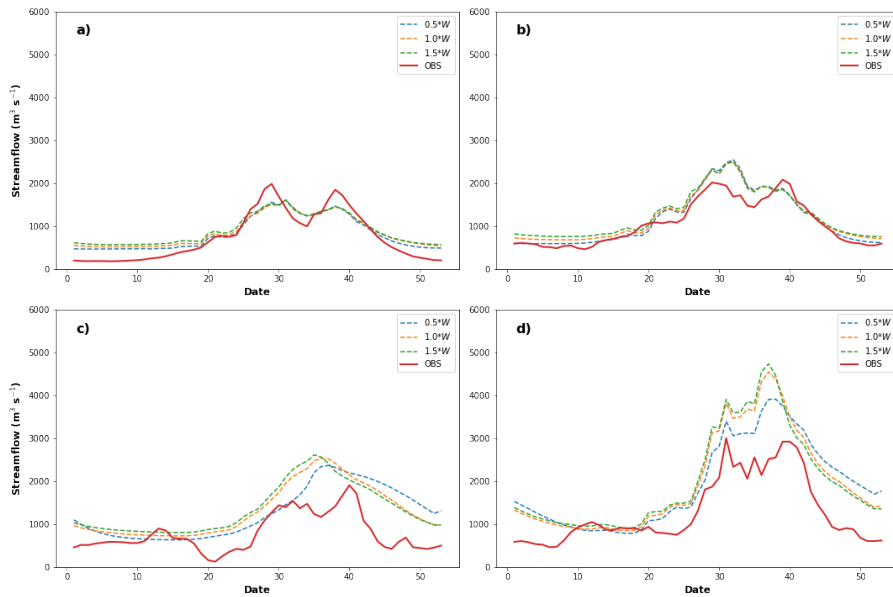


Figure A.3: Annual cycles of averaged weekly streamflow for the period of 1979-1988 at four main stations of Yellow River, Tangnaihe (a), Lanzhou (b), Toudaoguai (c) and Huayuankou (d), with the width of the river $W \times 0.5$ (blue), W (orange), $W \times 1.5$ (green), observed discharge (red).

Hydrological Modelling with Irrigation

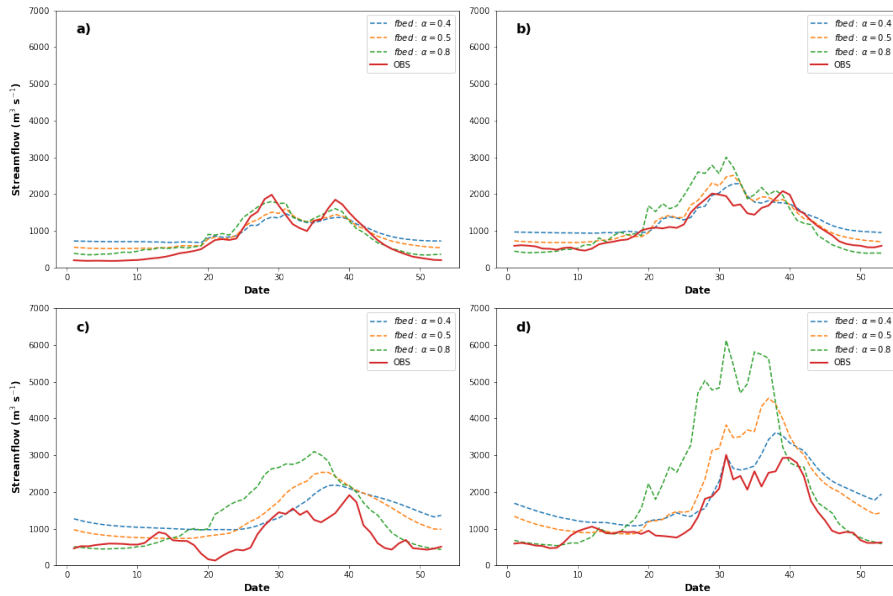


Figure A.4: Annual cycles of averaged weekly streamflow for the period of 1979-1988 at four main stations of the Yellow River, Tangnaihe (a), Lanzhou (b), Toudaoguai (c) and Huayuankou (d), with an exponent of the fraction of riverbed $\alpha=0.4$ (blue), 0.5 (orange), 0.8 (green), observed discharge (red).

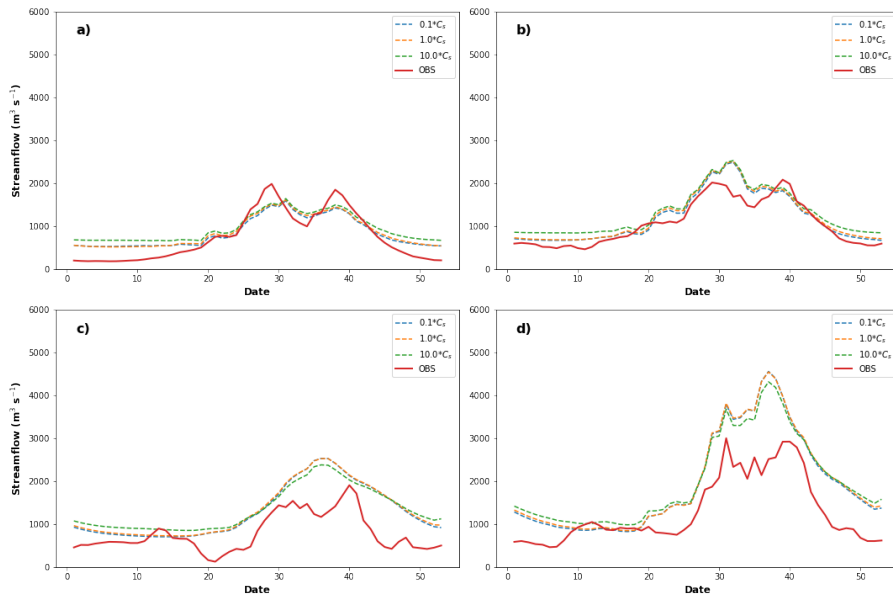


Figure A.5: Annual cycles of averaged weekly streamflow for the period of 1979-1988 at four main stations of the Yellow River, Tangnaihe (a), Lanzhou (b), Toudaoguai (c) and Huayuankou (d), with hydraulic conductance of stream-aquifer interconnection $C_s=0.4$ (blue), 0.5 (orange), 0.8 (green), observed discharge (red).